Electronic Supplementary Material

Individual gas sensor detecting dual exhaled biomarkers via a temperature modulated n/p semiconducting transition

Xiaxia Xing,[a] Lingling Du,[a] Dongliang Feng,[a] Chen Wang,[a] Mingshui Yao,[b] Xiaohu Huang,[c] Shixi Zhang,[d] and Dachi Yang *[a]

[a] Tianjin Key Laboratory of Optoelectronic Sensor and Sensing Network Technology and Department of Electronics, College of Electronic Information and Optical Engineering, Nankai University, Tianjin 300350, China

E-mail: yangdachi@nankai.edu.cn

[b] Institute for Integrated Cell-Material Sciences, Kyoto University Institute for Advanced Study, Kyoto University, Yoshida Ushinomio, Sya-chakyo-ku, Kyoto 606-8501, Japan

[c] Institute of Materials Research and Engineering, Agency for Science, Technology and Research, Singapore 138634

[d] Shangqiu Municipal Hospital, Shangqiu, 476100, China

Outline

Experimental section

Synthesis of $BiFeO_3/B_{25}FeO_{40}$ NPs

The schematic synthesis of $BiFeO_3/Bi_{25}FeO_{40}$ NPs is schematically descripted in Fig. S1. Firstly, 2.02 g $Fe(NO_3)_3 \cdot 9H_2O$ and 2.43 g $Bi(NO_3)_3 \cdot 5H_2O$ were dissolved in 10 mL nitric acid of 2 mol L^{-1}, and 6 mol L^{-1} KOH was dropped into above solution with stirring until no more precipitation appeared, then rinsed in deionized water until pH≈7 and the total volume of the solution is 80 mL. Secondly, 1g L^{-1} KNO_3 and 1.5g L^{-1} polyethylene glycol (PEG) were added under continuous stirring for 10 min. Thirdly, the solution was transferred into teflon-lined autoclave and was irradiated for 30 min at constant temperature (200 ^oC) and power (500 W) by a microwave hydrothermal instrument (XH-800G, Beijing Xianghu Technology Development Co., Ltd., China). Fourthly, the rufous powder was collected by filtering, washing in ethanol and deionized water thoroughly. The obtained samples were dried at 60 ^oC for 12 h in air-circulating oven (101-0AB, Tianjin Taisite Instrument Co., Ltd., China). Finally, the $BiFeO_3/Bi_{25}FeO_{40}$ NPs powder was obtained via annealing at 500 ^oC for 2 h in a muffle furnace (KSL1100X, Hefei Kejing Materials Technology Co. Ltd., China) with the heating rate of 2 ^oC min^{-1}.

Characterization

The as-obtained samples were characterized by field emission scanning electron microscopy (FE-SEM, JSM-7800) with energy dispersive X-ray spectroscopy (EDS, Oxford) and transmission electron microscopy (TEM, JEM-2200FS). X-ray diffraction (XRD) and high-resolution TEM (HRTEM, JEM-2200FS) were employed to obtain the crystalline properties of $BiFeO_3/Bi_{25}FeO_{40}$ NPs. X-ray photoelectron spectroscopy (XPS, Thermo Scientific ESCALAB 250Xi) was utilized to understand the chemical status of surface. The ultraviolet photoelectron spectroscopy (UPS, hermo Scientific ESCALAB 250Xi) and Ultraviolet-visible (UV-vis) absorption spectra (UV-Vis-NIR Spectrophotometer 5000) are conducted to determine the band structure of $BiFeO_3/Bi_{25}FeO_{40}$ NPs.

Testing method towards Mott-Schottky: [1]

Mott-Schottky testing was performed at an electrochemistry workstation (VersaSTAT 4, AMETEK Princeton) to obtain the nature of semiconductor. The details are descripted as follows. The measurements were performed in a three-electrode cell with 0.2 M Na_2SO_4 (PH

= 6.5) at the frequency of 1 kHz and the scan rate of 10 mV/s, where Pt wire serve as the counter electrode, and the Ag/AgCl electrode work as the reference electrode, respectively. The potential was measured against an Ag/AgCl reference electrode and converted to NHE potentials using E (NHE) = E (Ag/AgCl) + (0.059 × pH) + 0.197 V.

Gas sensing evaluations

Gas sensing test on the obtained $BiFeO_3/Bi_{25}FeO_{40}$ NPs was conducted by a static testing setup (WS-30B system, Weisheng Instruments Co. Ltd., Zhengzhou, China). The sensor prototypes were built similarly to previous investigations. [2, 3] Firstly, 50 mg $BiFeO_3/Bi_{25}FeO_{40}$ NPs were ground with terpineol, which was pasted around the surface of ceramic tube connected with Au electrodes and Pt wires. Then the tube was dried at 60 ^oC in an oven for 2 h. A Ni-Cr alloy wire as the heater, was inserted into the tube to control the working temperature. Finally, the sensor was aged for 24 h before the sensing evaluations. The sensing response is expressed by $S = R_a/R_g - 1$ (n-type mode) or $S = R_g/R_a - 1$ (p-type mode), where R_a and R_g are the resistances in the air and target gas, respectively. The response and recovery time are both defined as the time taken for the sensor to reach 90% of the initial resistance, in the case of injection or release of target gases, respectively. The relative humidity of the simulated breath in our case is ~72%.

Gas mixtures were obtained by mixing organic volatile gases and inorganic gases, respectively, which are then injected into the measuring chamber simultaneously for evaluating the sensing response. In our cases to evaluate the interferent selectivity of 5 ppm H_2S against 50 ppm interfering gases mixtures, (Group I) 50 ppm ethanol, acetone, toluene, and formaldehyde, and (Group II) 50 ppm CO, 50 ppm hydrogen and 5 ppm H_2S are mixed, respectively, then all above gases are injected into the measuring chamber. The gas distribution formula when measuring liquid vapor is shown as follows:

$$V_x = \frac{V \times C \times M}{V_m \times \rho \times \Phi} \times 10^{-6}$$

Where $V_x(\mu L)$ and $\mathrm{V}(mL)$ represent the volume of liquid and measuring chamber, $\mathrm{V} = 18\ \mathrm{L}$; C (ppm) and M (g/mol) are denoted as the concentration of target gas and the molecular weight of the liquid, respectively; ρ (g/mL) and ϕ are the density and purity of the liquid, respectively; $V_m(L/mol)$ refers to gas molar volume, under standard conditions, $V_m = 22.4\ L/mol$.

Human exhaled breath experiment

The experiments on detection of human breath were performed with the fully informed consent of the subjects.

Band structure

Generally, the band gaps of $BiFeO_3$ (JPCDS No. 86-1518) and $Bi_{25}FeO_{40}$ (JPCDS No. 46-0416) are 2.27 eV [4] and 1.94 eV, [5] respectively. Meanwhile, the conduction band minima (CBM) and valence band maxima (VBM) of the $BiFeO_3$ and $Bi_{25}FeO_{40}$ are theoretically analysed via following empirical equations. [6, 7]

$$E_{(CBM)} = \chi - E_e - 0.5\ E_g \quad (1)$$

$$E_{(VBM)} = E_{(CBM)} + E_g \quad (2)$$

Where χ is the geometric average of the absolute electronegativity of the constituent atoms, the pearson absolute electronegativity of Bi, Fe and O atoms are about 4.69, 4.06 and 7.54 eV, respectively, [8] and E_e is the energy of a free electron in hydrogen scale which is approximately 4.5 eV. Therefore, {CBM, VBM}s of $BiFeO_3$ and $Bi_{25}FeO_{40}$ were calculated to be {0.42 V, 2.69 V} and {0.77 V, 2.71 V} (vs. NHE) respectively, which implies that CBM and VBM of $Bi_{25}FeO_{40}$ are more positive than those of $BiFeO_3$, and thus a type-II band alignment is formed within $BiFeO_3$-$Bi_{25}FeO_{40}$ interface when an equilibrium is reached. [9]

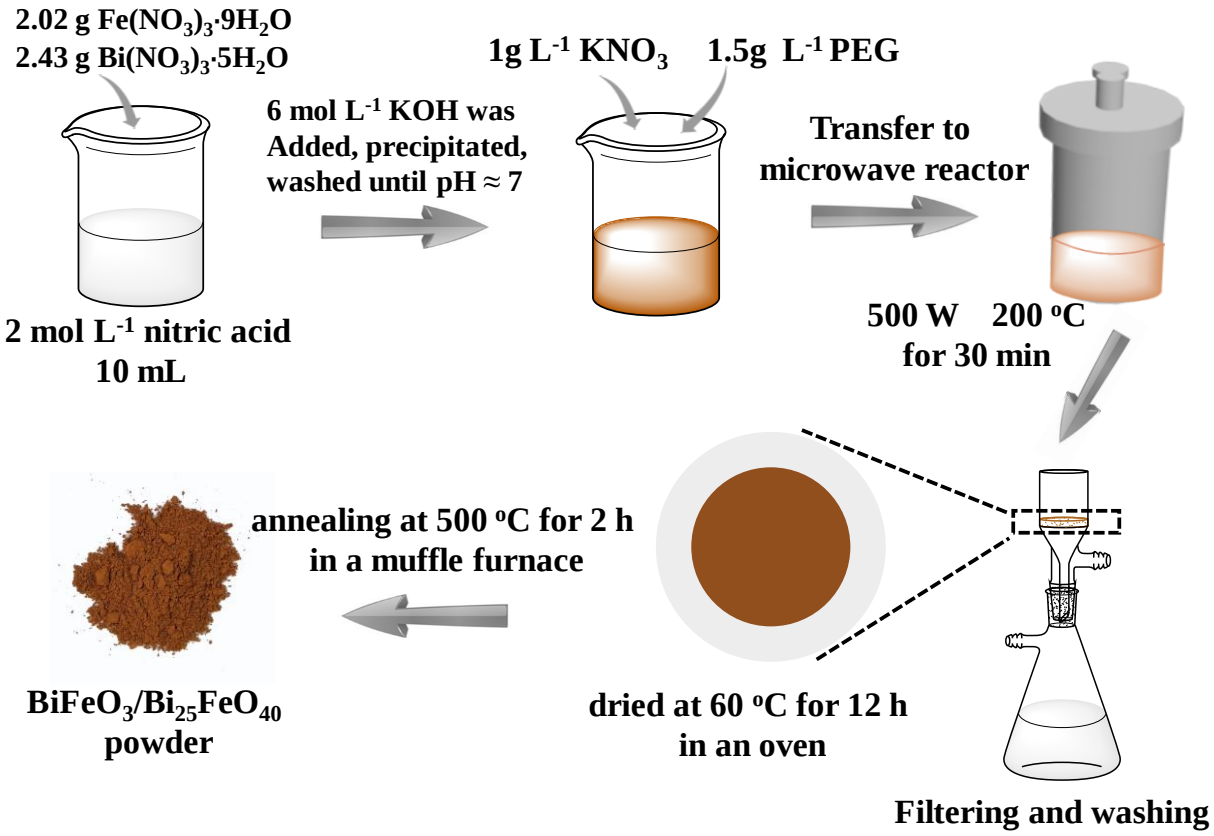

Fig. S1 Schematic synthesis of interconnected $BiFeO_3/Bi_{25}FeO_{40}$ NPs.

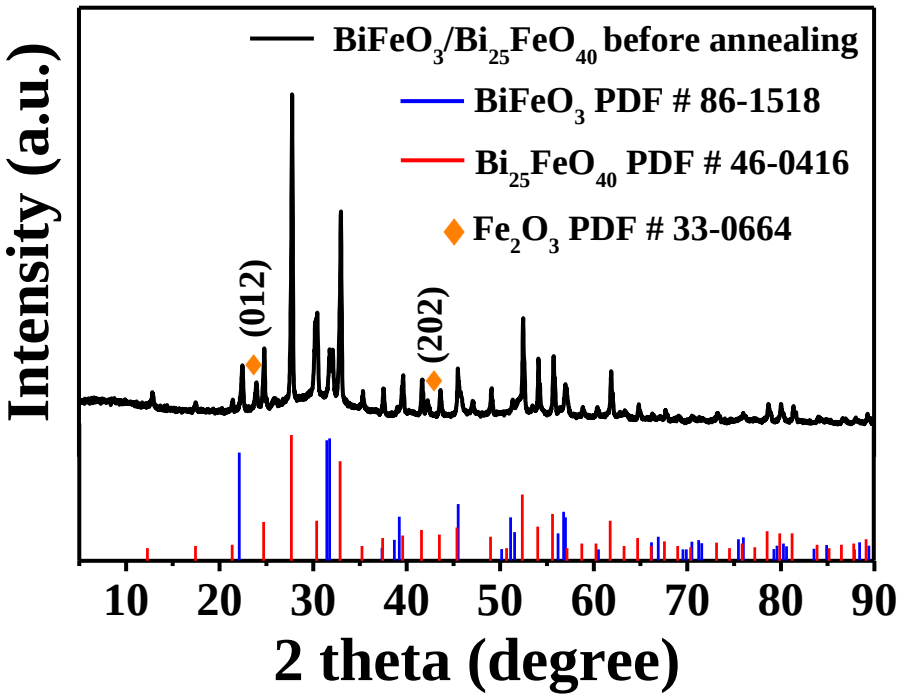

Fig. S2 XRD pattern of $BiFeO_3/Bi_{25}FeO_{40}$ NPs before annealing.

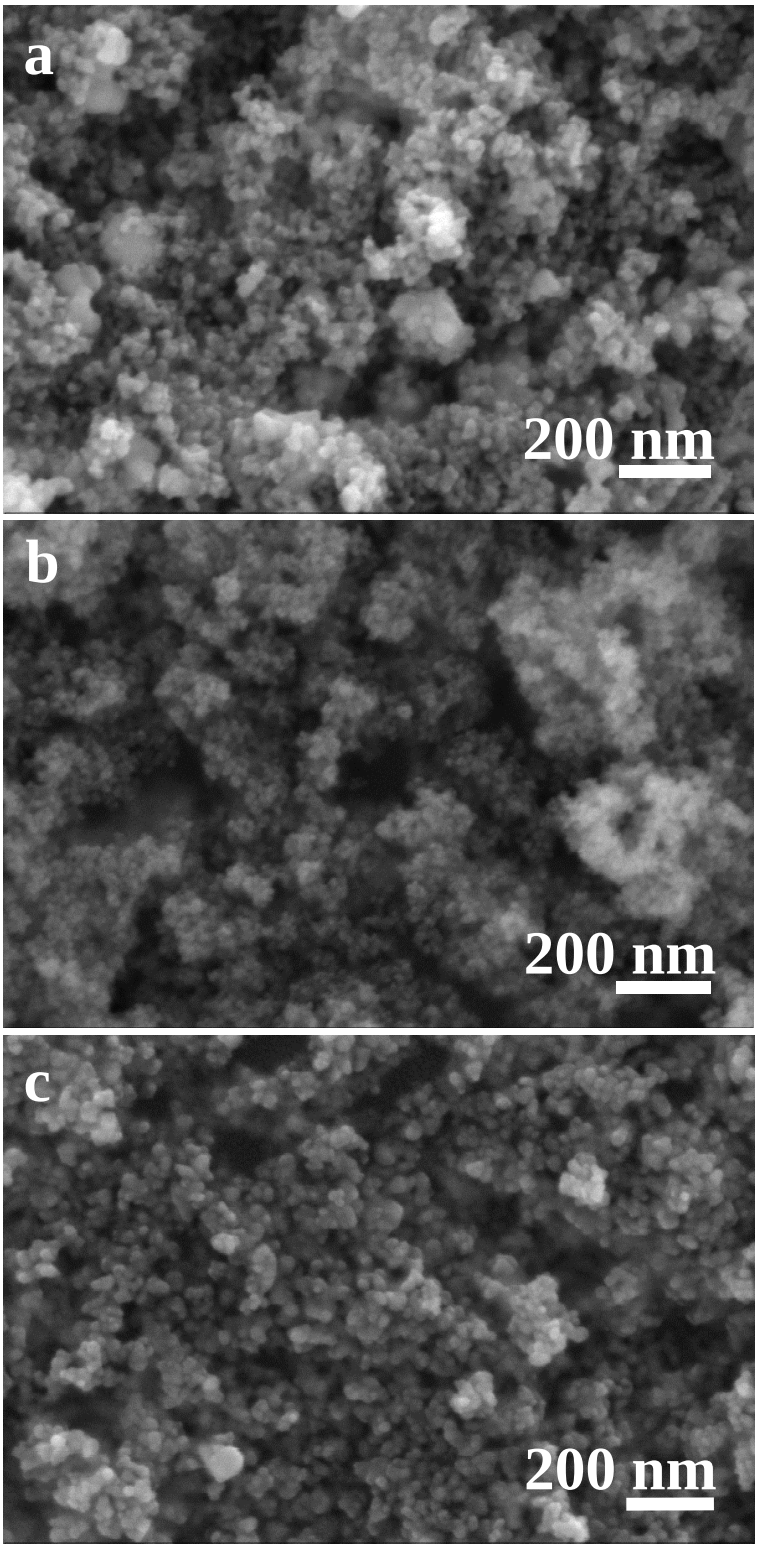

Fig. S3 The SEM images of $BiFeO_3/Bi_{25}FeO_{40}$ NPs obtained with various precursors. The SEM images of $BiFeO_3/Bi_{25}FeO_{40}$ NPs with (a) 1g/L KNO_3, (b) 2g/L KNO_3, (c) 2g/L KNO_3 and 1.5g/L PEG are added in precursor, respectively.

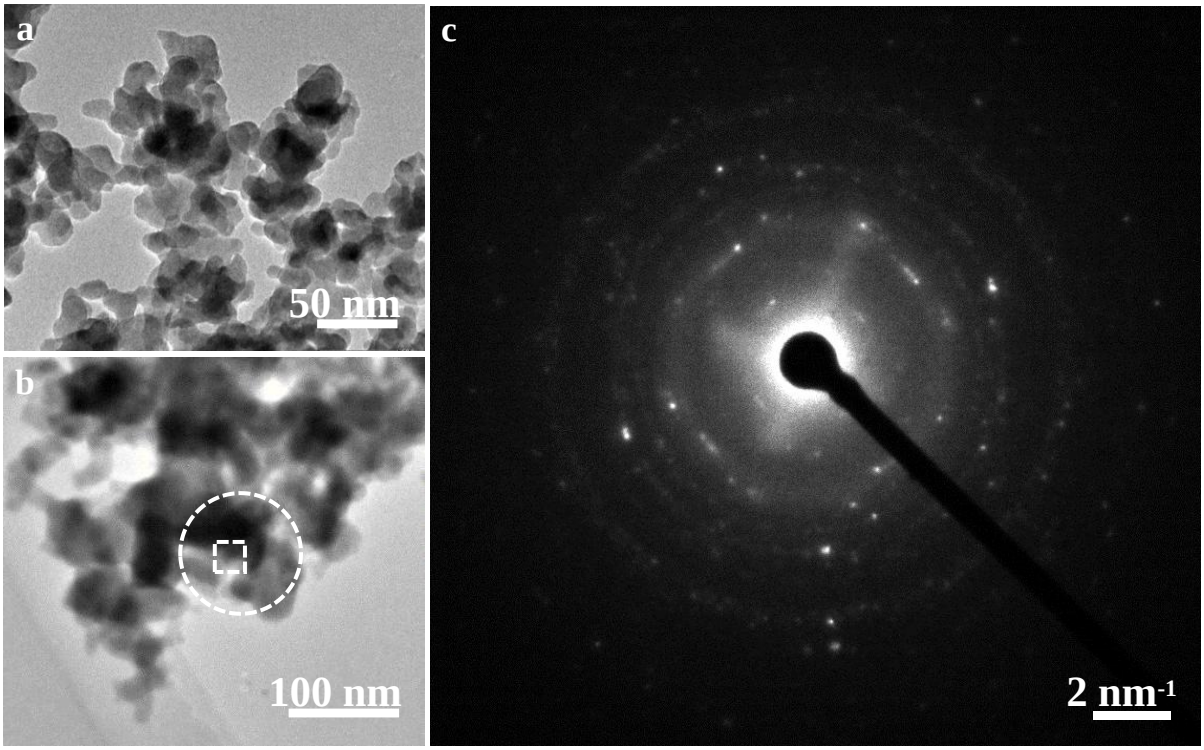

Fig. S4 More detailed TEM characterizations of $BiFeO_3/Bi_{25}FeO_{40}$ NPs. (a) The enlarged TEM images of $BiFeO_3/Bi_{25}FeO_{40}$ NPs corresponding to Fig. 1 b in the manuscript. (b) The corresponding region for HRTEM image of Fig. 1 d and the SAED pattern of Fig. 1 e. (c) The raw SAED pattern corresponding to Fig. 1 e of the manuscript.

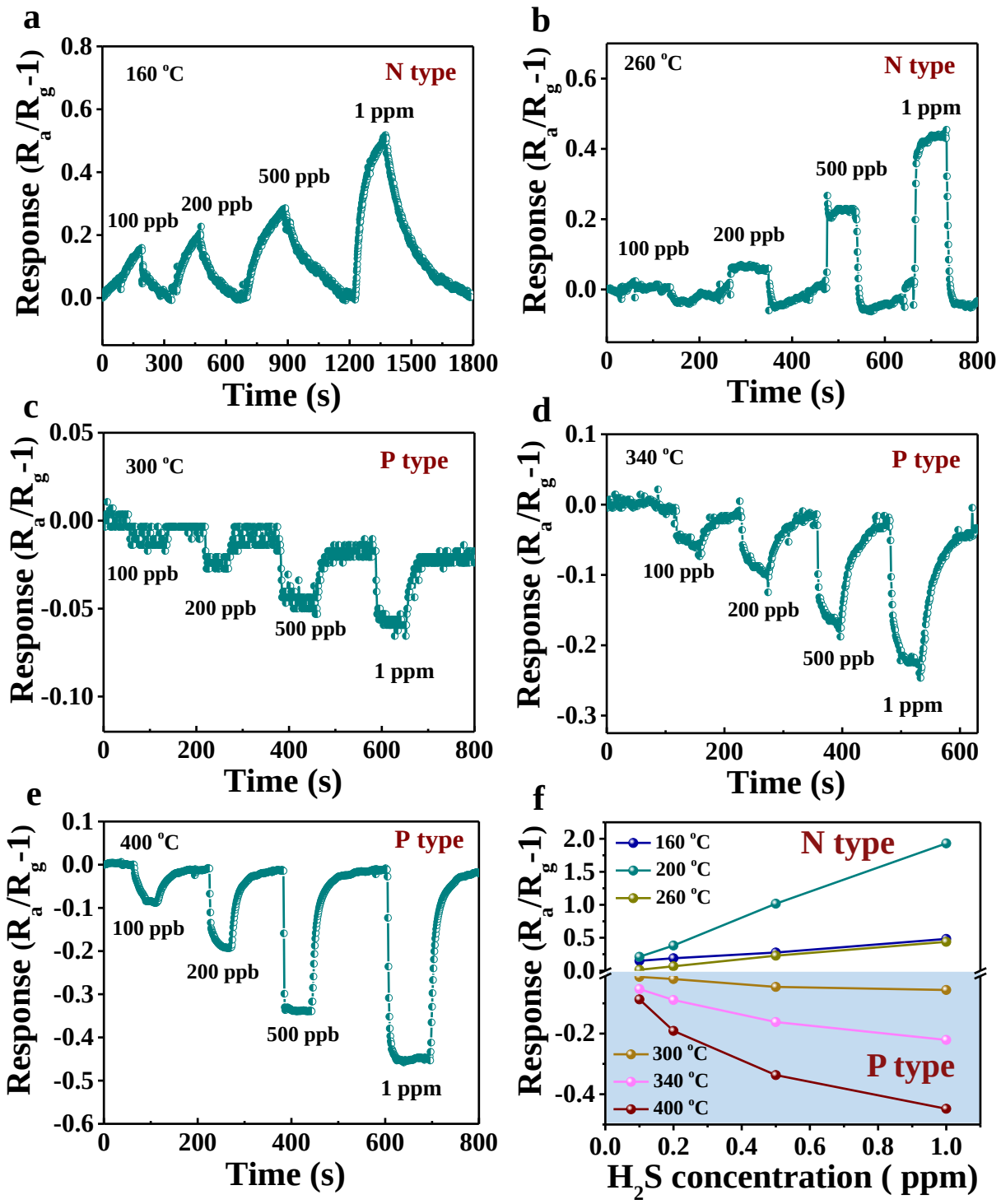

Fig. S5 The responses of the $BiFeO_3/Bi_{25}FeO_{40}$ NPs sensor prototype towards 0.1-1 ppm H_2S at the working temperatures of (a) 160 °C, (b) 260 °C, (c) 300 °C, (d) 340 °C, and (e) 400 °C. (f) The summarized responses plots. The relative humidity (RH) of above test is of ~ 30%.

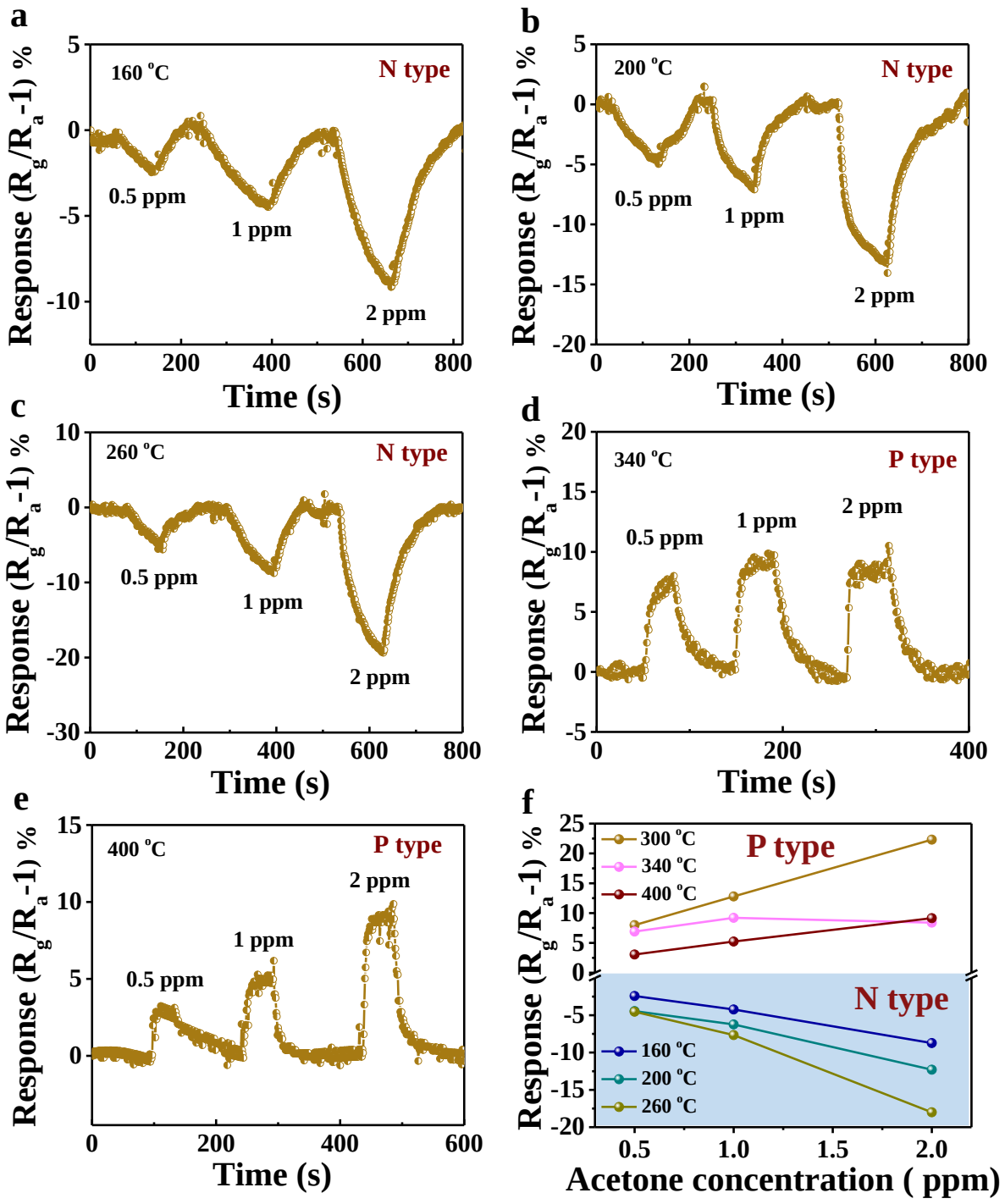

Fig. S6 The responses of the $BiFeO_3/Bi_{25}FeO_{40}$ NPs sensor prototype towards 0.5-2 ppm acetone at the working temperatures of (a) 160 °C, (b) 200 °C, (c) 260 °C, (d) 340 °C, and (e) 400 °C. (f) The summarized responses plots. The relative humidity (RH) of above test is of ~ 30%.

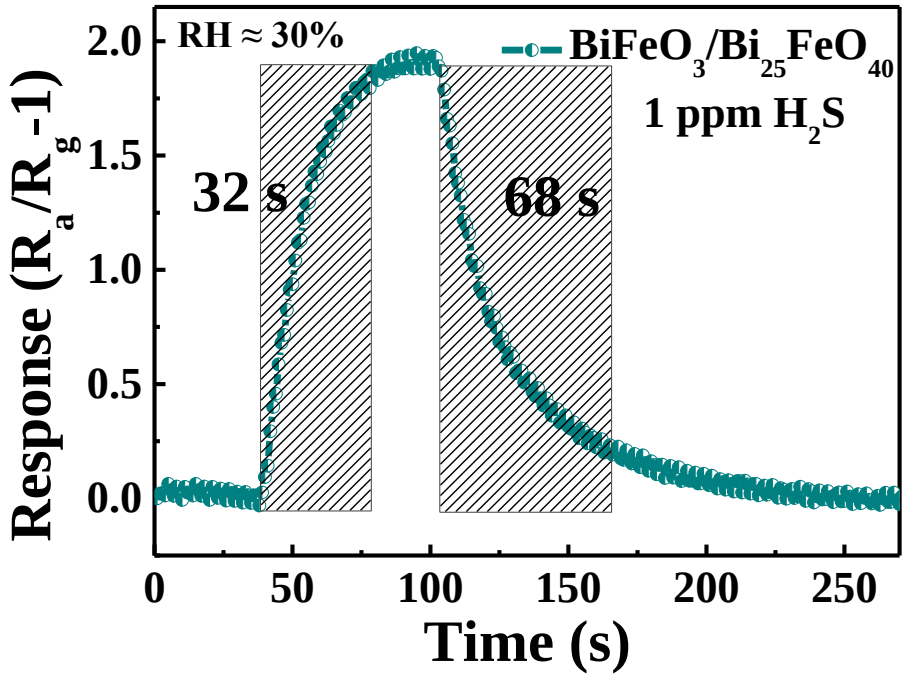

Fig. S7 The response/recovery time of $BiFeO_3/Bi_{25}FeO_{40}$ NPs to 1 ppm H_2S under n-type mode at 200 °C.

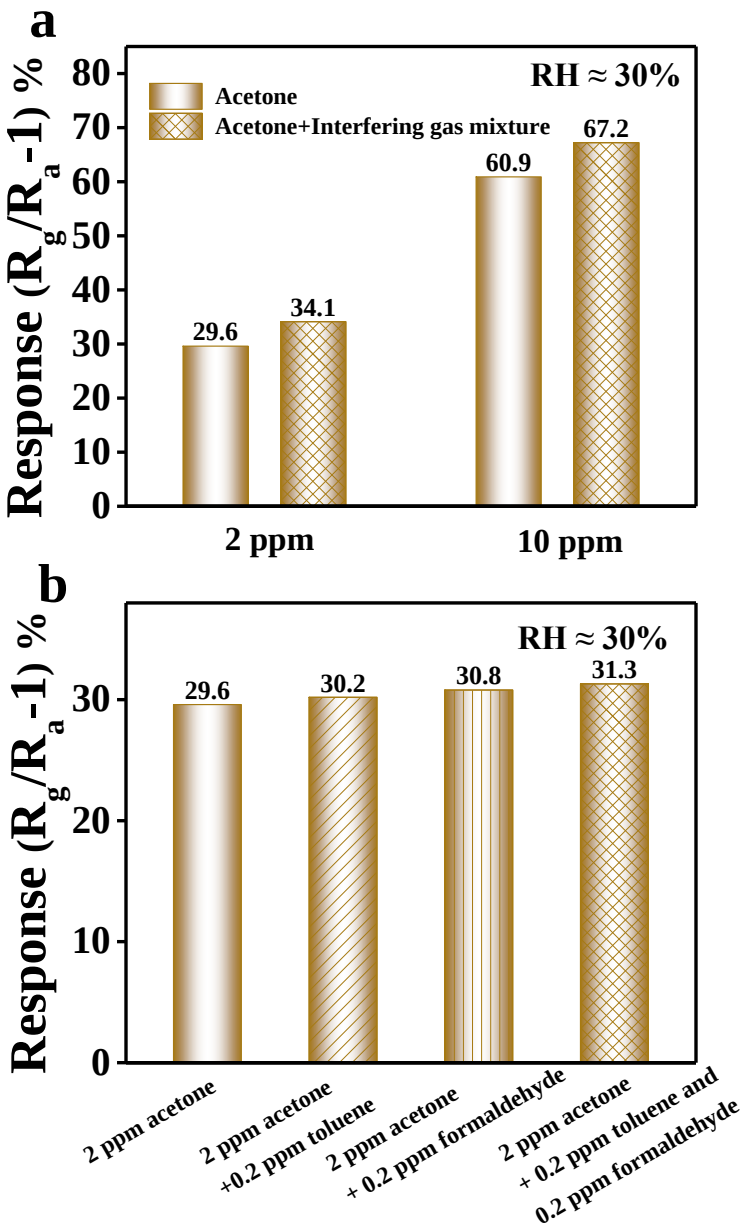

Fig. S8 Interferent selectivity evaluation of $BiFeO_3/Bi_{25}FeO_{40}$ NPs under p-type mode. (a) Comparison of the sensitivities towards single acetone and its mixture with interfering gases. Interfering gas mixtures include toluene, formaldehyde, CO, H_2, and H_2S, of which the concentration is applied the same as that of target acetone. (b) The interferent selectivity of $BiFeO_3/Bi_{25}FeO_{40}$ NPs against toluene and formaldehyde.

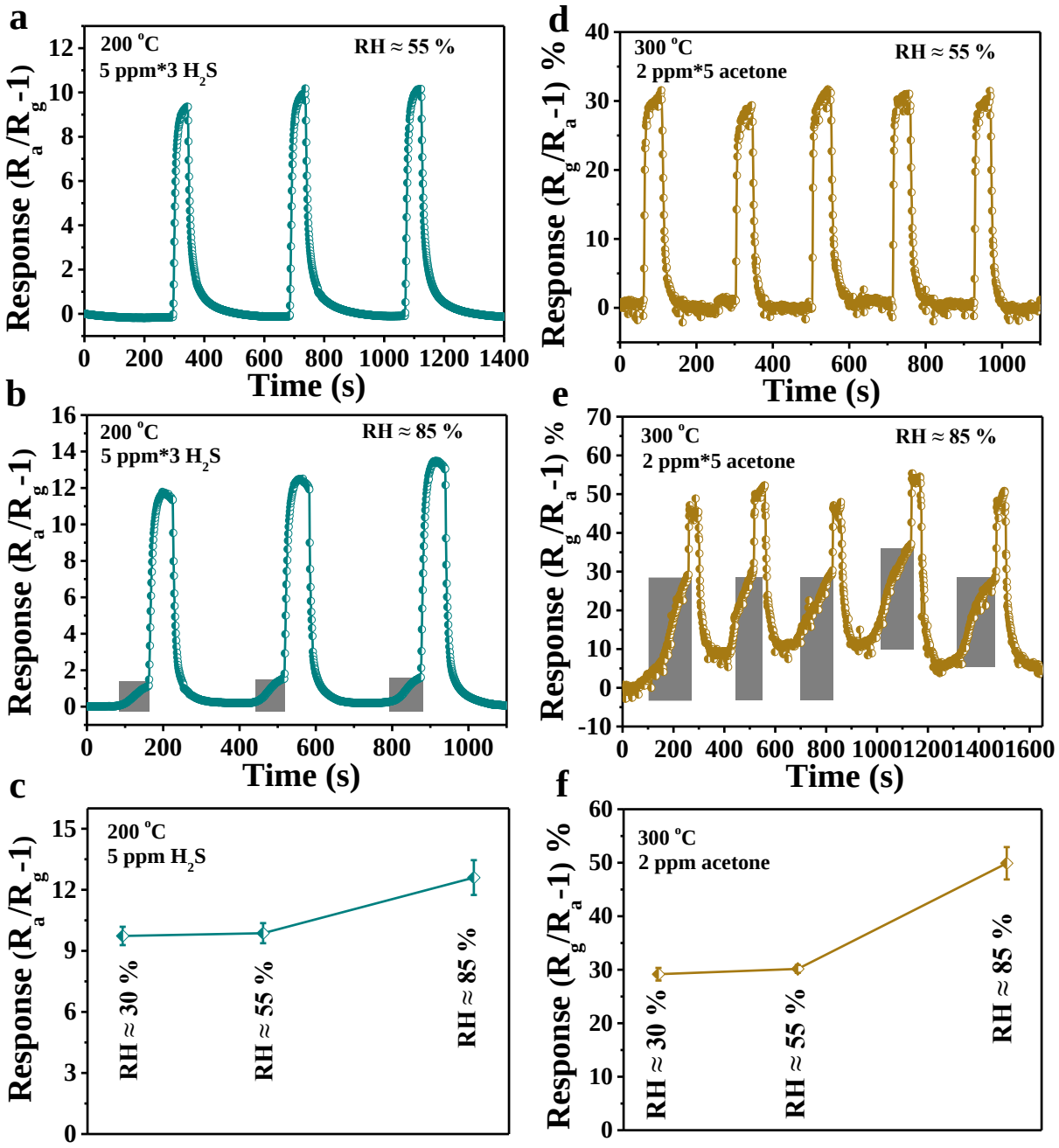

Fig. S9 The response of $BiFeO_3/Bi_{25}FeO_{40}$ NPs under n-type and p-type mode at different relative humidity. The plots of real-time response to 5 ppm H_2S at (a) RH≈55% and (b) RH≈85%. The plots of real-time response to 2 ppm acetone at (d) RH≈55% and (e) RH≈85%. (c, f) Comparison of response under various humidity. The curves marked with gray boxes in (b) and (e) represent the influence of humidity.

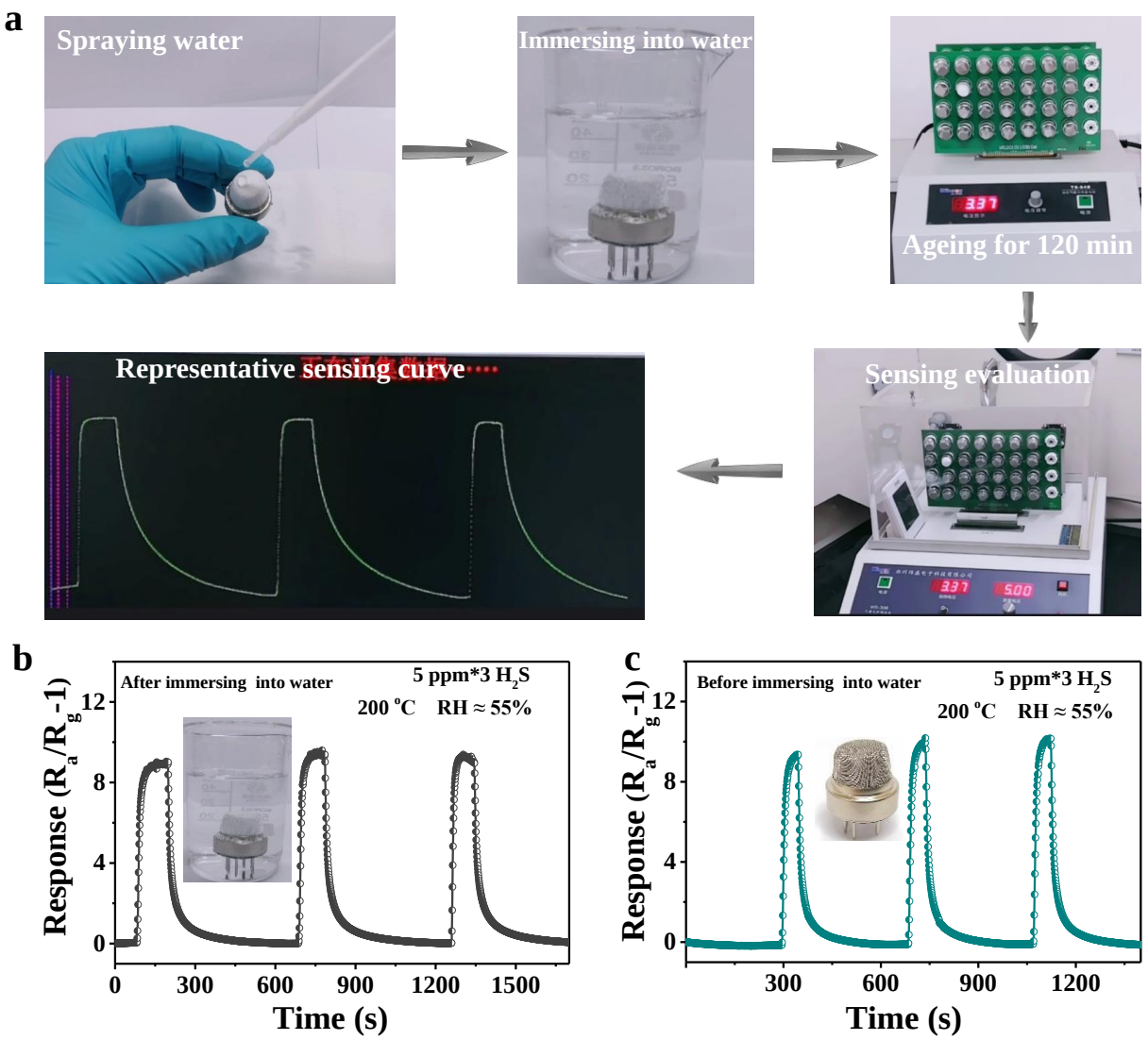

Fig. S10 The gas sensing performance evaluation of the sensor prototype with waterproof. (a) The sensor was tested under critical conditions of spraying and immersing into water. (b) The real-time response plot of the sensor covering waterproof membrane being immersed in deionized water for 120 min was compared with the same sensor (c) without waterproof one.

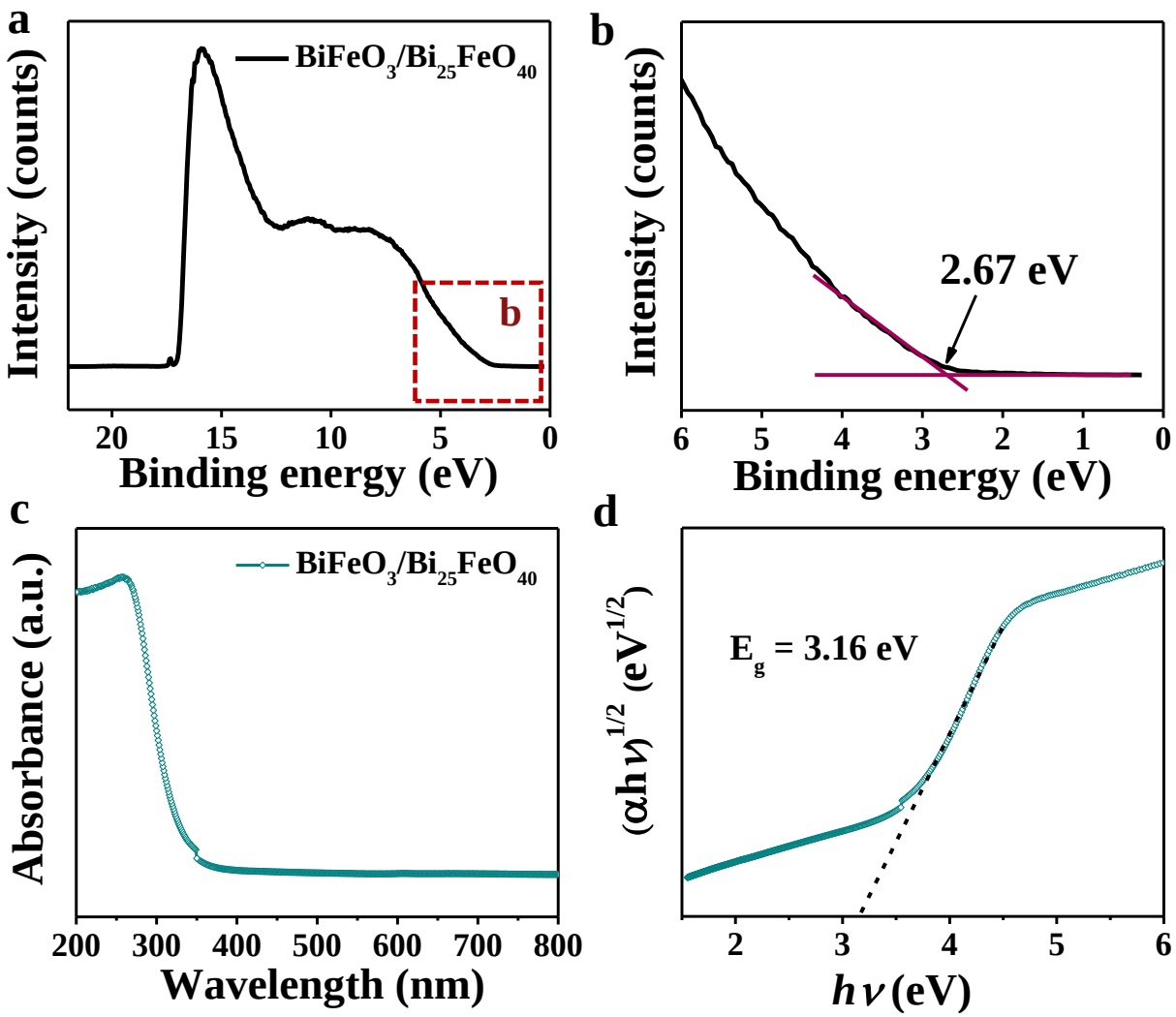

Fig. S11 (a) UPS valence band spectra of $BiFeO_3/Bi_{25}FeO_{40}$ NPs. Energies are referenced to the Fermi level (0 eV). (b) Amplified valence band spectrum of $BiFeO_3/Bi_{25}FeO_{40}$ NPs to determine the maximum valence band. (c) UV–vis absorbance spectra of $BiFeO_3/Bi_{25}FeO_{40}$ NPs, (d) band gap determination from $(\alpha h\nu)^{1/2}$ versus ($h\nu$) plot.

UV-vis absorption spectra. The band gap values (E_g) of $BiFeO_3/Bi_{25}FeO_{40}$ NPs can be estimated using a plot of $(\alpha h\nu)^{1/2}$ versus ($h\nu$) according to the equation expressed as $\alpha h\nu = A(h\nu - E_g)^{n}$, where α, $h\nu$, E_g, and A are denoted as absorption coefficient, photon energy, band gap, and a constant, respectively. Herein n equals 2 for indirect band gap semiconductor oxide. [4]

Table S1. Gas sensing performance of the $BiFeO_3$-based sensors in previous publications.

$BiFeO_3$-based samples	**Target gases**	**Conc. (ppm)**	**Res. (R_g/R_a or R_a/R_g)**	**Temp. (^oC)**	**Low Detection limit (ppm)**	**Ref**
$BiFeO_3$ nanoparticles and nanosheets	Acetone	10	14.98	500	1	[10]
Walnut-shaped $BiFeO_3$ microspheres	Formaldehyde	500	8.2	240	2	[11]
$BiFeO_3$ nanoparticles	acetone	10	12	350	1	[12]
La-Bi-Fe-O nanorod	Formaldehyde	50	23.3	100	5	[13]
$BiFeO_3$ nanoparticles	SO_2	5	2.03	300	-	[14]
$BiFeO_3$ /$Bi_{0.9}Ba_{0.1}FeO_{2.95}$	Ethanol	100	5 14	400	5 -	[15]
$BiFeO_3$ nanoparticles	CO	30	2.12	350	5	[16]
$BiFeO_3/Bi_{25}FeO_{40}$ interconnected nanoparticles	**H_2S** **Acetone**	**10** **10**	**25.1 (10 ppm)** **63.3% (10 ppm)**	**200** **300**	**0.1** **0.5**	**This work**

References

1 Y. Wang, L. Liu, C. Meng, Y. Zhou, Z. Gao, X. Li, X. Cao, L. Xu, W. Zhu, *Sci. Rep.,* 2016, **6**, 33092.

2 Z. Zhu, L. Zheng, S. Zheng, J. Chen, M. Liang, Y. Tian, D. Yang, *J. Mater. Chem. A,* 2018, **6**, 21419-21427.

3 Z. Zhu, L. Zheng, S. Zheng, J. Chen, X. Xing, D. Feng, D. Yang, *J.Mater. Chem. A,* 2019, **7**, 10456-10463.

4 H. You, Z. Wu, L. Zhang, Y. Ying, Y. Liu, L. Fei, X. Chen, Y. Jia, Y. Wang, F. Wang, S. Ju, J. Qiao, C.-H. Lam, H. Huang, *Angew. Chem. Int. Ed.*, 2019, **58**, 11779-11784.

5 G. Wang, D. Cheng, T. He, Y. Hu, Q. Deng, Y. Mao, S. Wang, *J. Mater. Sci: Mater. El.,* 2019, **30**, 10923-10933.

6 A. H. Nethercot, *Phys. Rev. Lett.*, 1974, **33** , 1088-1091.

7 X. Li, T. Wan, J. Qiu, H. Wei, F. Qin, Y. Wang, Y. Liao, Z. Huang, X. Tan, *Appl. Catal. B: Environ.*, 2017, **217** , 591-602.

8 R. G. Pearson, *Inorg. Chem.*, 1988, **27**, 734-740.

9 W. Li, X. Wu, J. Chen, Y. Gong, N. Han, Y. Chen, *Sens. Actuators, B,* 2017, **253**, 144-155.

10 Y. Zhang, H. Xu, S. Dong, R. Han, X. Liu, Y. Wang, S. Li, Q. Bu, X. Li, J. Xiang, *J. Mater. Sci. Mater. El.,* 2018, **29**, 2193-2200.

11 K. M. Zhu, S. Y. Ma, S. T. Pei, Y. Tie, Q. X. Zhang, W. Q. Wang, X. L. Xu, *Mater. Lett.,* 2019, **246**, 107-110.

12 S. Chakraborty, M. Pal, *J. Alloy. Compd.,* 2019, **787**, 1204-1211.

13 Q.-J. Ruan, W.-D. Zhang, *Mater. Lett.,* 2008, **62**, 4303-4305.

14 S. Das, S. Rana, S. M. Mursalin, P. Rana, A. Sen, *Sens. Actuators, B,* 2015, **218**, 122-127.

15 G. Dong, H. Fan, H. Tian, J. Fang, Q. Li, *RSC Adv.,* 2015, **5**, 29618-29623.

16 S. Chakraborty, M. Pal, *New J. Chem.,* 2018*,* **42***,* 7188-7196*.*